Mixing Enhancement/Suppression of Separated-and-Reattaching Flow by an Upstream Small Object

Yusuke IINUMA, Department of Mechanical Engineering, Doshisha University, Kyoto 610-0321, Japan
Jiro FUNAKI, Department of Mechanical Engineering, Doshisha University, Kyoto 610-0321, Japan, jfunaki@doshisha.ac.jp
Katsuya HIRATA, Department of Mechanical Engineering, Doshisha University, Kyoto 610-0321, Japan, khirata@doshisha.ac.jp

Keywords: Separated-and-Reattaching Flow, Mixing Enhancement, Mixing Suppression, Heat Transfer, Semi-Infinite Plate, Flow Control, Bluff Body, Shear Layer

1. Introduction

Generally, flow around a bluff body such as a circular cylinder is complicated compared with that around a streamlined body because of the existence of separated shear layers. Long bluff body such as a flat blunt plate is more complicated than short bluff body, because of separated-and-reattaching flow on the after bodies.

Control methods have been suggested variously. One of the methods is to insert a small control object around the body, where main aim was originally drag reduction due to the change of separated share layers. This method is expected to be affective on drag reduction, mixing enhancement/suppression and vibration suppression. There have been some previous reports concerning the control object around a circular cylinder[1)&2)], a square cylinder[3)&4)], or a rectangular cylinder[5)&6)] in order to changes the forming position and area of the Karman vortex street behind the body.

However, as is mentioned earlier, streamwise long body flow is different from short body one, such as circular and square cylinders, because shear layer separated from a leading edge reattaches the surfaces, namely, separated-and-reattaching flow is formed. One of the simplest bodies that bring separated-and-reattaching flow is a semi-infinite plate. Kiya et al.[7)] and Sasaki & Kiya[8)] researched the effect on separated-and-reattaching flow of an upstream small object, and reported (1) shorter reattaching length, (2) thinner separated shear layer and (3) weaker pressure fluctuation on the plate surface. They mentioned that their main reason is the effect on separation points of free-stream turbulence from the small control object.

In the present study, we progress the above studies.[7)&8)] Namely, a circular or a square cylinder as a control object is placed in the upstream of a semi-infinite plate. Then, our purpose is to specify a position effect and a size effect of the control object. We conducted (1) velocity-fluctuation measurements in a wind tunnel at a Reynolds number Re of 5000 and (2) numerical analyses at Re=1500.

Nomenclature

d	:	Diameter of circular control object m
f	:	Dominant frequency of velocity-fluctuation $=1/T$ Hz
H	:	Semi-infinite plate thickness m
l	:	Distance from plate leading edge to control object center m
Re	:	Reynolds number (based on length scale H) $=U_0H/\nu$
s	:	Side length of square control object m
$St(l)$	:	Strouhal number (based on length scale l) $=fl/U_0$
T	:	Dominant period of velocity-fluctuation s
t	:	Time s
U	:	Time-mean velocity m/s
U_0	:	Velocity of main flow m/s
u'	:	R.M.S. value of velocity m/s
u_1'	:	R.M.S. value of velocity near plate separation point m/s
u'_{max}	:	Maximum R.M.S. value of velocity in separated share layer m/s
x	:	Streamwise distance from plate leading edge m
y	:	Cross-streamwise center from plate center m
ν	:	Kinetic viscosity m^2/s
ρ	:	Density kg/m^3

2. ExperimentalApparatus and Method

2-1. ExperimentalApparatus

Experimental apparatus for the present study is depicted in Fig. 1. Experiments are performed in an closed-return, low-speed wind tunnel with a 1m high, 1m wide and 2m long test section. The turbulence level in the empty test section is less than 0.5% at the speed of 5m/s. A tested semi-infinite plate has an aspect ratio W/H of 20 (W is the width of the plate) and a chord-to-thickness ratio L/H of 25 (L is the length of the plate).The plate is made of acrylic resin. Endplates with $10H$ height, $1H$ width and $37.5H$ length are attached at both ends of the plate. Blockage ratio of the plate to a nozzle exit of the wind tunnel is 0.0088. Tested control objects tested are 8 circular cylinders of d/H=0.05~0.4 and 2 square cylinders of s/H=0.25, 0.35.

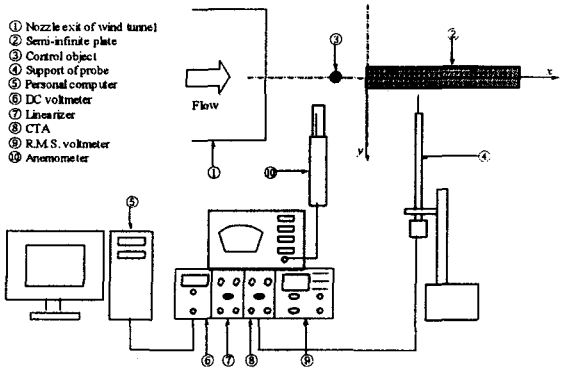

Fig. 1 Experimental apparatus.

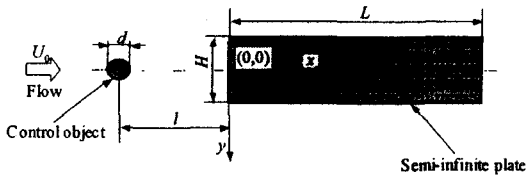

(a) Circular control object

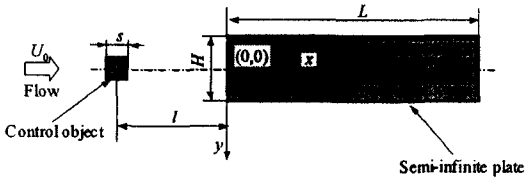

(b) Square control object

Fig. 2 Coordinate system and objects.

2-2. Experimental Method

The coordinate system is shown in Fig. 2; the x-axis is streamwise, the$y$-axis is cross-streamwise (downward positive), and the origin is at the center of the leading blunt face. Flow velocity is measured by a hot-wire anemometry with an I-probe whose position is specified as (x,y). l is the distance from the plate to the control object. A prove support is insert perpendicular to main flow. Running power spectrum analyses of velocity-fluctuation are conducted in a personal computer. Measured dominant frequency is non-dimensionalised as the Strouhal number.

3. Computational Theory

3-1. Governing Equations

If flow velocity is much lower than sonic in gas flow, fluid motion is governed by the incompressible Navier-Stokes equations. The Reynolds number is defined as

$$Re = \frac{U_0 H}{\nu}. \tag{3.1}$$

The incompressible Navier-Stokes equations are

$$\nabla \cdot \boldsymbol{V} = 0 \tag{3.2}$$

and

$$\frac{\partial \boldsymbol{V}}{\partial t} + (\boldsymbol{V} \cdot \nabla)\boldsymbol{V} = -\nabla p + \frac{1}{Re}\Delta \boldsymbol{V}. \tag{3.3}$$

Here, $\boldsymbol{V}$ is velocity vector, ∇ is gradient operator, and Δ is Laplacian. Equation (3.2) is continuity equation and equation (3.3) is the Navier-Stokes equation. These are governing equations for the present study. The governing equations (3.2) and (3.3) are transformed to following basic equations, because our solving method is a finite deference method, namely, MAC method.

$$\Delta p = -\nabla \cdot \{(\boldsymbol{V} \cdot \nabla)\boldsymbol{V}\} + \frac{(\nabla \cdot \boldsymbol{V})^n}{\Delta t} \tag{3.4}$$

and

$$\frac{\partial \boldsymbol{V}}{\partial t} + (\boldsymbol{V} \cdot \nabla)\boldsymbol{V} = -\nabla p + \frac{1}{Re}\Delta \boldsymbol{V}. \tag{3.5}$$

All space derivatives are discretised by second-order central finite differences and time integral method is first-order explicit Euler's method.

3-2. Computational Conditions

Computational grids are two-dimensional rectangle with variable sizes. Grid points are 837 in the streamwise and 257 in the cross-streamwise. Mesh system is staggered one. Initial conditions are u=1, v=0, and p=0 at all points. Computational field $x_N \times y_N$=74.061H $\times$23.163H, minimum mesh size $\Delta x=\Delta y=H/40$, and plate lengthx_B=61.037H. The control object in numerical analyses has square cross section of s/H=0.35. We compute till non-dimensional time 250, where 100 is enough log to simulate. Time-step Δt is 0.0005.

4. Results and Discussion

4-1. R.M.S. Value of Velocity near Separation Point

Wake turbulence behind the control object is a function of position, and is also affected by the existence of the semi-infinite plate. Therefore, measurement position for turbulence should be decided appropriately. Here, our probe position is the same as Kiya et al.[7] They suppose that shear layer turbulence near flow separation point is the most essential factor to affect separated-and-reattaching flow characteristics. Their and our position $(x,y)=(0,0.55H)$.

Fig. 3 shows contour lines of the R.M.S. value u_1' at $(x,y)=(0,0.55H)$, as a function of position and size of the circular control object. Here, × and a chain line represent a ridge, which corresponds a local maximum of u_1'. ● is experimental u_1' at Re=26000, by Kiya et al.[7] From this figure, we can classify flow into 2, mode A and mode B.

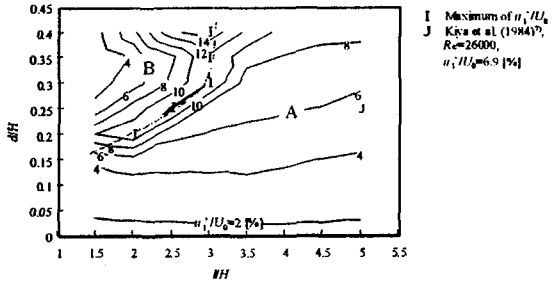

Fig. 3 Contour line of R.M.S. value of velocity u_1' (Circular control object).

4-2. Strouhal Number

To determine dominant frequencies and the Strouhal numbers, we conduct running spectrum analyses. A control object is a circular cylinder. Probe position is at x=1H and y=0.1H~0.5H from the object center, that corresponds to the inside of wake behind the object. This position is the best place to get clear spectrum peaks. A sample of running power spectrum profiles for d/H=0.35 is shown in Fig. 4. Fig. 4(a) is in mode A, and shows one spectrum peak, Fig 4(b) is in mode B, and one or two peaks depending on time. Hereafter, dominant frequencies f are non-dimensionalised as the Strouhal number. Dominant frequencies from the object without the plate are measured as x=1.5H and y=0.3H from the object center.

Fig. 5 shows an example of Strouhal number measurements. Here, an abscissa is l/H, and an ordinate is $St(l)$, which is the Strouhal number based on l instead of H as length scale. ○ is asymptotic to the Karman-vortex-shedding frequencies (solid line). ● is mostly

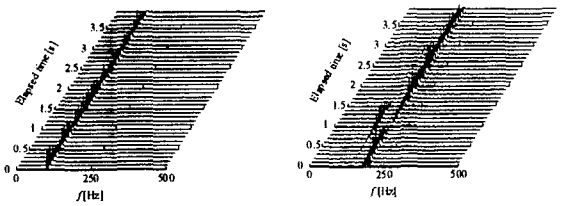

(a) l/H=4.0 in mode A (b) l/H=2.5 in mode B

Fig. 4 Running power spectrum profile with circular control object d/H=0.35 (Reference position is x=1.5H, y= 0.5H from control object).

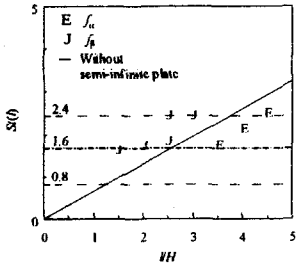

Fig. 5 Strouhal number $St(l)$ against position of circular control object d/H=0.35.

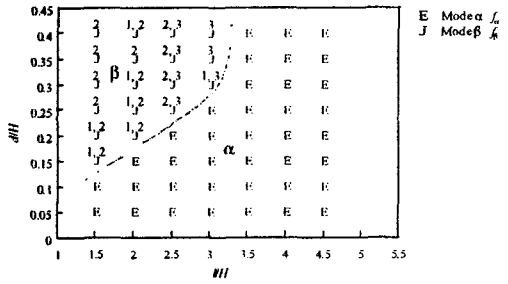

Fig. 6 Occurrence territory of Strouhal number $St(l)$ (Circular control object).

constant against l/H, the values are almost in multiples of 0.8. Then, the phenomenon is similar to the edgetone[9]. Hereafter, former is called mode α and latter is mode β. Fig. 6 shows distribution of mode a and b on l/H-d/H plane. From this figure, it is proved when the object is not far from the plate, $St(l)$ is constant, and the dominant frequency depends on size of the object. Moreover, the boundary between mode α and mode β is very close to that between mode A and mode B. Then, the flow-mode classification based on the R.M.S. value is closely related with that based on the $St(l)$.

4-3. Velocity Measurements on Surface of Semi-Infinite Plate

Velocity measurements near the sideface of the plate are summarised in Fig. 7 in order to compare characteristics of shear layers. In general, the control

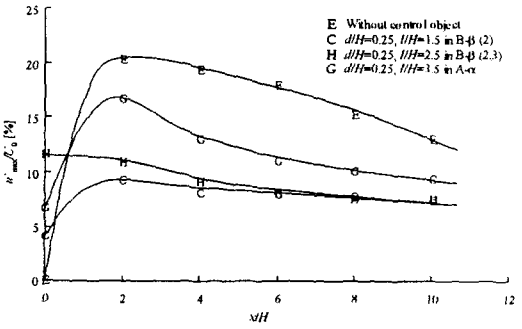

Fig. 7 Distribution maximum R.M.S. value of velocity u'_{max} by circular control object.

object can suppress turbulence intensity level of shear layers. Especially in mode B-β, turbulence suppression is significant.

4-4. Verification of Computational Accuracy

In Fig. 8, we compare experimental and computational results of $St(l)$. The control object has square cross section of s/H=0.35. Here, solid and broken lines are the Karman-vortex-shedding frequencies without the plate at Re=5000 and 1500, respectively. Computational results f_α at l/H=2.5, 3.0, 4.0 are asymptotical to a broken line with increasing l/H. Computational results at l/H=1.5~2.5 show the feature that $St(l)$ is almost fixed to the value of 0.8 independently to l/H. As a result, our computation is successfully simulates the phenomenon, qualitatively.

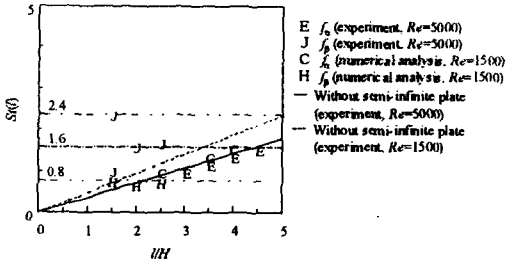

Fig. 8 Comparison between experiments and computations on Strouhal number $St(l)$ (Square control object, s/H=0.35).

4-5. Flow Pattern

Flow pattern near the object and the plate can be observed in detail by numerical analyses. Here, our aim is to research the relatively between mode α and mode β. Fig. 9 shows vorticity-density patterns for s/H=0.35 and l/H=2.5 Fig. 9(a) is in mode α, and Fig. 9(b) is in mode β. Wave length of mode α, namely, the interval of vortices, is shorter than that of mode β, corresponds to the results in Fig. 8. Remarkable difference between

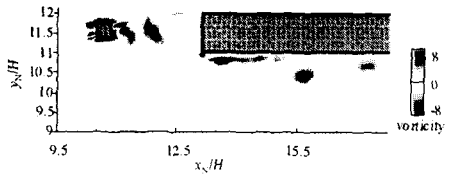

(a) Mode α

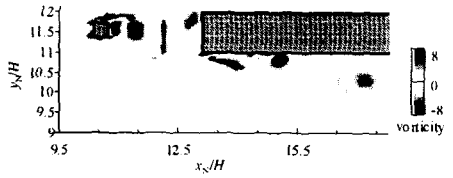

(b) Mode β(1)

Fig. 9 Flow pattern with control object at 2/4T (s/H=0.35, l/H=2.5, numerical analysis, Re=1500, density of vorticity).

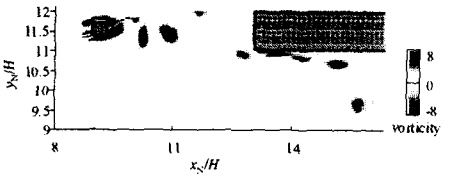

(a) Discharge of single vortex

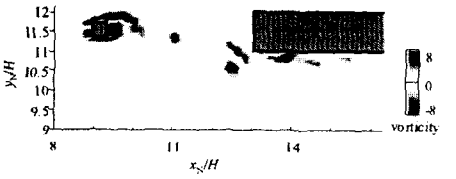

(b) Discharge of pair of vortices

Fig. 10 Flow pattern with control object (s/H=0.35, l/H=4.0 in mode α, numerical analysis, Re=1500, density of vorticity).

Fig. 9(a) and Fig. 9(b) is shown on the front of the plate; that is, in mode β, vortices hit the plate front and distort. Fig. 10 shows the result for s/H=0.35 and l/H=4.0 in order to study mode α. In Fig. 10(a), we can see discharge of single vortex and in Fig. 10(b), discharge of a pair of vortices toward edge. Periodicity of mode α is clearer than that of mode β.

5. Conclusions

In the present study, flow around the semi-infinite plate with an upstream control object was researched by experimental velocity-fluctuation measurements and numerical analyses. The main results can be summarized as follows.

(1) We can classify the flow into 2, namely, mode A and

mode B, based on the R.M.S. value of velocity.

(2) We can classify the flow into 2, namely, mode α and mode β, based on the dominant frequency of velocity-fluctuation.

(3) The flow-mode classification based on the R.M.S. value of velocity is closely related with that based on the non-dimensional frequency of velocity.

(4) The control object tends to suppress turbulent intensity of separated shear layers. The suppressed effect is more efficient in mode B-β than mode A-α.

(5) We observed different-mode flow patterns of mode α and modeβ by numerical analyses.

References

1) Igarashi, T. and Tsutsui, T.: Flow Control Around a Circular Cylinder by a New Method (1st Report), *Trans. JSME B*, **55** (511), 1989, pp. 701-707 (in Japanese).

2) Tan, K., Sakamoto, H. and Moriya, M.: Suppression of Fluid Forces of a Circular Cylinder by Passive Control of Flow, *Trans. JSME B*, **68** (674), 2002, pp. 2772-2779 (in Japanese).

3) Sakamoto, H., Haniu, H. and Obata, Y.: An Optimum Suppression of Fluid Forces by Controlling the Separated Shear Layer, *Trans. JSME B*, **55** (520), 1989, pp. 3622-3629 (in Japanese).

4) Iwata, Y. and Morishita, E.: Numerical Study of Passive Flow Control Around a Rectangular Cylinder, *Trans. JSME B*, **68** (673), 2002, pp. 2504-2510 (in Japanese).

5) Igarashi, T. and Terachi, N.: Drag Reduction of Flat plate Normal to Airstream, *Trans. JSME B*, **61** (589), 1995, pp. 3114-3121 (in Japanese).

6) Tan, K., Sakamoto, H., Takai, K. and Haniu, H.: Suppression of Fluid Forces of Rectangular Cylinders by Passive Control of Flow, *Trans. JSME B*, **64** (622), 1998, pp. 1772-1780 (in Japanese).

7) Kiya, M., Sasaki, K. and Arie, M.: Effect on Free-Stream Turbulence on a Separation Bubble, *Trans. JSME B*, **50** (452), 1984, pp. 967-973 (in Japanese).

8) Sasaki, K. and Kiya, M.: Effect on Free-Stream Turbulence on Turbulent Properties of a Separation-Reattachment Flow, *Bull. JSME*, **28** (238), 1985, pp. 610-616.

9) Rockwell, D. and Gartshore, I. S.: Self-Sustained Oscillations of Impinging Free Shear Layers, *Ann. Rev. Fluid Mech.*, **11**, 1979, pp. 67-94.